JACS
JOURNAL OF THE AMERICAN CHEMICAL SOCIETY
Communication
pubs.acs.org/JACS

Tuning the Light Emission Properties by Band Gap Engineering in Hybrid Lead Halide Perovskite

Valerio D'Innocenzo,[†,‡] Ajay Ram Srimath Kandada,*[,†] Michele De Bastiani,[†,§] Marina Gandini,[†] and Annamaria Petrozza*[,†]

[†]Center for Nano Science and Technology @Polimi, Istituto Italiano di Tecnologia, via Giovanni Pascoli 70/3, 20133 Milano, Italy
[‡]Dipartimento di Fisica, Politecnico di Milano, Piazza L. da Vinci 32, 20133 Milano, Italy
[§]Dipartimento di Scienze Chimiche, Università degli studi di Padova, Via Marzolo 1, 35122 Padova, Italy

Supporting Information

ABSTRACT: We report about the relationship between the morphology and luminescence properties of methylammonium lead trihalide perovskite thin films. By tuning the average crystallite dimension in the film from tens of nanometers to a few micrometers, we are able to tune the optical band gap of the material along with its photoluminescence lifetime. We demonstrate that larger crystallites present smaller band gap and longer lifetime, which correlates to a smaller radiative bimolecular recombination coefficient. We also show that they present a higher optical gain, becoming preferred candidates for the realization of CW lasing devices.

After revolutionizing the field of photovoltaics, organometal halide perovskites are also emerging as viable materials for light-emitting devices, paving the way toward solution-processable and tunable electrically pumped lasers.[1−3,31] This increases the interest in the understanding of the optical properties of these materials. Recent works have demonstrated that the photoluminescence (PL) decay in $CH_3NH_3PbI_3$ ($MAPbI_3$) thin films can be described by simple rate equations involving carrier trapping and electron−hole radiative recombination. In particular, according to Yamada et al.,[4] Stranks et al.,[5] and Saba et al.[6] the PL dynamics are driven by a radiative nongeminate electron−hole recombination process,[7] possibly also involving nonradiative de-excitation paths. Thus, the temporal evolution of the excited carrier population $n(t)$ can be satisfactorily modeled by taking into account a bimolecular intrinsic radiative recombination coefficient ($B_{rad} = R_{rad}/n_i^2$, where R_{rad} is the radiative rate and n_i is the intrinsic carrier concentration) and a nonradiative monomolecular trapping rate (A), i.e., $dn/dt = -An - B_{rad}n^2$. At low excitation densities the charge-trapping pathways limit the PL quantum efficiency, whereas at high fluences the traps are predominantly filled and recombination of the photogenerated species is dominated by efficient radiative processes. This explains well the increase in the PL quantum efficiency at higher fluences.[1,5]

Another notable phenomenon is the incredibly long PL lifetime found for the *Cl-doped* $MAPbI_3$, which reaches up to hundreds of nanoseconds, especially because it has been associated with photocarrier diffusion lengths of micrometers.[8] Such a long lifetime was initially associated with the presence of Cl^- ions within the perovskite unit cell. However, recent investigations have highlighted a major role of the chlorine-based precursor in the crystallization process of the hybrid perovskite. In particular, some of us have shown that Cl is not present in detectable concentrations in the unit cell and is mainly expelled from the flat films. Nevertheless, its presence drives the crystallization dynamics, producing larger crystals with anisotropic shape.[9] This highlights an important unexplored issue of the relationship between structural and optoelectronic properties in these self-assembled compounds. Hybrid perovskites are usually deposited as polycrystalline thin films with variable mesoscale morphologies that depend on the growth conditions.[10,11] The obtained grain size ranges from tens to thousands of nanometers depending on the processing method, and this seems to strongly influence the solar cell performance,[10,12] though such observations have never been fully rationalized.

Here we investigate the influence of the morphology of the $MAPbI_3$ thin film, from a molecular to mesoscopic level, on the luminescence properties. Figure 1a−d shows top-view scanning electron microscopy (SEM) images of four representative samples investigated in this work, with an observed average size of the crystallite dimension ranging from <250 nm to >2 μm. They were fabricated using the two-step sequential deposition technique[13,14] (for a detailed description of the protocol, see the Supporting Information (SI)). The top panel of Figure 1e shows the positions of the optical band edges obtained from UV−vis absorption spectra as well as the positions of the PL peaks for all of the samples (associated SEM images and spectra of the entire set of samples are shown in Figures S1 and S2 in the SI, respectively). We observe that as the polycrystallite grows in size, the optical absorption edge shifts to longer wavelengths (lower energies) along with the PL peak position, keeping constant the shift between the two.

Figure 1f shows the time-resolved PL (tr-PL) dynamics of the aforementioned series of samples. The measured tr-PL decays were fit with a stretched exponential function to obtain the respective PL lifetimes, which are reported as a function of the average crystallite size in the bottom panel of Figure 1e (for details, see the SI). For the smallest crystals (<250 nm), we obtained a lifetime of about 2 ns. As the crystallite size was

Received: November 5, 2014
Published: December 3, 2014

dx.doi.org/10.1021/ja511198f | J. Am. Chem. Soc. 2014, 136, 17730−17733

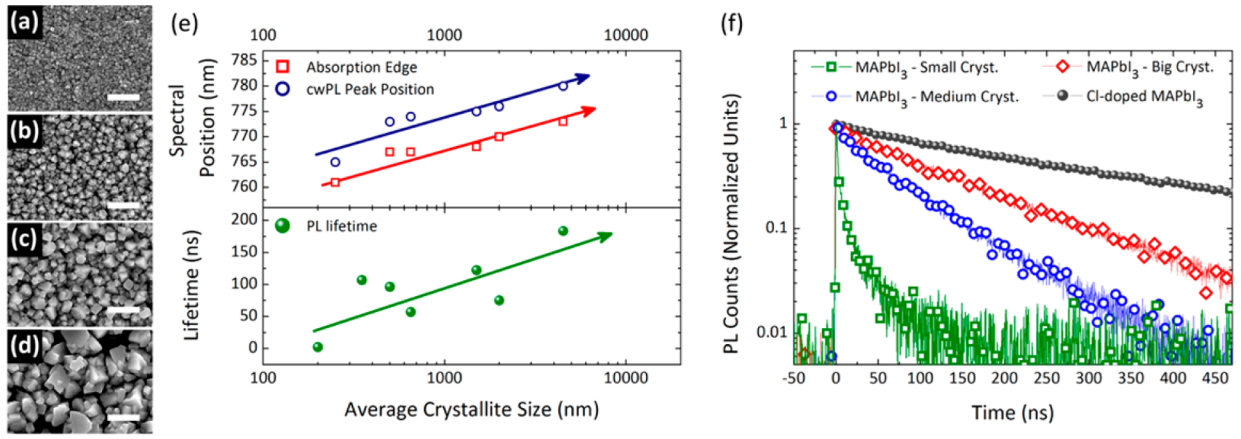

Figure 1. (a–d) Top-view SEM images of $MAPbI_3$ formed using (a) [MAI] = 0.063 M, T = 25 °C; (b) [MAI] = 0.045 M, T = 25 °C; (c) [MAI] = 0.031 M, T = 25 °C; (d) [MAI] = 0.045 M, T = 70 °C. Scale bars are 2 μm. (e) (top) Spectral positions of the UV–vis absorption band edge and cw-PL peak position and (bottom) PL lifetime as functions of the crystallite size (SEM images of the full set of samples are reported in Figure S1). (f) Representative tr-PL dynamics for three different $MAPbI_3$ crystal sizes and PL dynamics of Cl-doped $MAPbI_3$ spin-coated on a glass substrate. The pump wavelength was 700 nm, and the initial excitation density was ~4 × 10^{16} cm^{-3}.

increased, we observed an associated increase in the lifetime (Figure 1e, bottom panel), with the largest crystallites (>1 μm) showing a lifetime greater than 100 ns, approaching values that in previous works have been reported only for Cl-doped $MAPbI_3$ samples[8,15] (reported in Figure 1f as black circles for comparison).

Our results show that the PL lifetime critically depends on the specific morphology of the sample and thus on the adopted fabrication protocol.[8,11,15−17] At this stage, the most intuitive conclusion may suggest an enhancement of the nonradiative channels when the polycrystallinity increases. In order to shed light on such observations, we first needed to validate the use of the model proposed by Yamada et al.[4] for the set of samples considered here. Specifically, we needed to exclude any nonradiative bimolecular mechanisms such as surface recombination. Figure 2a shows the excitation density dependence of the normalized PL yield[6] for the sample with the smallest crystallites, which would be most likely to present a larger number of surface defects (see Figure S4 in SI for the results for larger crystals). The efficiency increases with increasing excitation density, thus supporting a major role of radiative recombination in the bimolecular recombination process also in the small crystallites. It must be noted that above a certain threshold (excitation density > 10^{17} cm^{-3}) density-dependent nonradiative processes become more important and eventually dominate, causing the decrease of the PL yield. Saba et al.[6] modeled this behavior according to Auger-like mechanisms proportional to n^3. Interestingly, smaller crystallites present a lower threshold for such nonradiative mechanisms compared with larger crystals (see Figure S4) and Cl-doped $MAPbI_3$.[6] This may be related to the presence of higher defect densities in the smaller crystallites.[18]

Figure 2b shows the excitation density dependence of the PL lifetimes. Two representative samples were chosen, the one studied in Figure 2a with <250 nm crystallites and $MAPbI_3$ with >1 μm crystallites, corresponding to the samples shown in Figure 1a,d, respectively. In this framework, the dependence of the PL lifetime on the initial excitation density (n_0) can be written as[4,19]

$$\tau_{PL} = (A + B_{rad} n_0)^{-1} \quad (1)$$

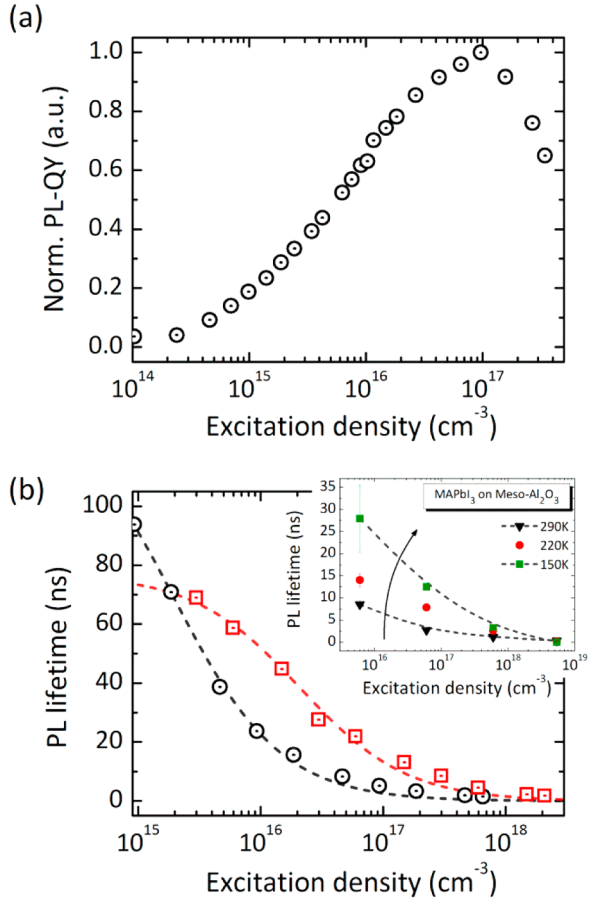

Figure 2. (a) Normalized PL quantum yield (calculated as the ratio of the integrated PL spectrum to the incident power) for the sample shown in Figure 1a. (b) PL lifetime as a function of the excitation density for $MAPbI_3$ samples with small (black circles) and large (red squares) crystallites. Dashed lines represent the curves obtained fitting the data to eq 1. The inset shows the PL lifetime as a function of initial excitation density for Meso-$MAPbI_3$ at room temperature (black triangles), 220 K (red circles), and 150 K (green squares). The error bars refer to the 95% confidence intervals of the fitted parameter values.

dx.doi.org/10.1021/ja511198f | J. Am. Chem. Soc. 2014, 136, 17730−17733

By fitting eq 1 to the experimental data, we estimated the intrinsic bimolecular radiative recombination coefficient for both samples. We found that the larger crystallites exhibit a lower radiative recombination coefficient, $B_{rad} = (0.62 \pm 0.06) \times 10^{-9}$ s^{-1} cm^3, with respect to the smaller ones, $B_{rad} = (3.7 \pm 0.2) \times 10^{-9}$ s^{-1} cm^3, and this indeed results in the longer PL lifetimes (Saba et al. found $B_{rad} = 0.25 \times 10^{-9}$ s^{-1} cm^3 for a Cl-doped $MAPbI_3$ flat film). It should be noted that the monomolecular trapping rate A is not very much affected, decreasing from 1.3×10^7 s^{-1} to 0.72×10^7 s^{-1} as the crystallite dimension decreases. However, this rate is usually very sensitive to the sample production process.[4,19,20] It may be associated with localized defects in the crystals and thus may vary significantly from sample to sample as a result of imperfect control of their fabrication.

As noticed above, the reduction in B_{rad} is accompanied by a red shift of the band edge, which goes from 1.63 eV in the case of the small crystallites to 1.61 eV for the large crystallites, showing a correlation between E_g and B_{rad}. Intensity-dependent PL measurements as the sample temperature was lowered also corroborated this observation. It has been previously observed that as the temperature is lowered (while staying above the temperature for the phase transition[21,22]), the optical band gap of the perovskite shifts to lower energies as a consequence of lattice stress (Varshni shift[23]). In this case, we considered a $MAPbI_3$ film deposited by the two-step procedure on a 1 μm thick Al_2O_3 mesoporous scaffold (denoted as Meso-$MAPbI_3$ in the following). Here the presence of the scaffold assured a crystal size smaller than 50 nm,[9] allowing us to exclude excitonic effects even at lower temperatures.[21] We observed a PL lifetime of about 2 ns when the sample was excited with a density comparable to the one used to obtain the PL decay shown in Figure 1f ($\sim 6 \times 10^{16}$ cm^{-3}). At that initial excitation density (i.e., fixed laser fluence), as the temperature was decreased, the PL lifetime increased and the spectra shifted to longer wavelengths (Figure S3). The inset of Figure 2b shows the plots of the PL lifetime versus the excitation density at different temperatures. Considering again eq 1 and looking at the slopes of the emissive recombination rates (evaluated as $1/\tau_{PL}$) plotted versus excitation density (see also Figure S5b in SI), it is clear a decrease of Brad (which is proportional to that slope) as the temperature is lowered. Hence, the correlation between E_g and B_{rad} observed by increasing the crystal dimension can also be perceived by lowering the temperature, which notably affects the lattice strain, suggesting a direct relation between the two.

Mitzi and co-workers experimentally demonstrated that in 2D tin-based hybrid perovskite semiconductors, the relaxation of the halide−metal−halide bonding angle induced by different arrangements of the organic plays a fundamental role in the determination of the electronic structure of these materials.[24] In agreement, very recently theoretical studies revealed that it is possible to modulate the optical gap of $MAPbI_3$ perovskites over almost an electron volt by modulating the Pb−I−Pb bond angle without altering the metal−halide chemistry.[25,26] These theoretical findings find support in the Raman analysis by Grancini and co-workers, which revealed a stronger distortion in the Pb−I bond in moving from large crystals grown on a flat substrate to smaller crystals grown in a mesoporous scaffold.[9,27] Thus, we relate the observed shrinkage of the optical band gap in the larger perovskite crystallites to a change in the Pb−I bond stress. In a recent work, Filippetti et al.[28] showed by ab initio calculations that different orientation patterns of the organic cation within the perovskite lattice correspond to distinct equilibrium energy states associated with a shift of the energy gap of the semiconductor. Importantly, they highlight a dependence of B_{rad} on the optical band gap of $MAPbI_3$ perovskites. In particular, they associate the reduction in B_{rad} with a reduction in the band gap due to the direct dependence of the radiative recombination rate R_{rad} and the intrinsic carrier concentration n_i on the band gap.[29]

Thus, we conclude that controlling the crystallization procedure allows the semiconductor band gap and the intrinsic radiative lifetime of the compound to be engineered. In view of the potential employment of these materials for lasing applications, it is interesting at this stage to understand how one can exploit simple processing to optimize the emissive properties of the thin film. A longer lifetime would create a larger steady-state population under continuous-wave (cw) illumination, which can be beneficial for low-threshold cw lasing. However, another important parameter that determines the lasing threshold is the gain coefficient of the material, which is related not only to the recombination rates but also to the nonradiative losses. To shed light on this aspect, we performed optical gain measurements using the established variable stripe length method[30] (for details, see the SI). Briefly, the spatial profile of the photoexcitation is made into a stripe, and the emission is collected from one end of the stripe. The output intensity $I(\lambda, l)$ is then related to the stripe length l by

$$I(\lambda, l) = \frac{A(\lambda) I_p}{g(\lambda)} [e^{g(\lambda) l} - 1] \quad (2)$$

where A is a constant related to the spontaneous emission cross section, I_p is the intensity of the pump, g is the gain coefficient, and λ is the emission wavelength. The PL intensities from the two samples with large and small crystallites as functions of stripe length at three different powers along with the fits obtained using eq 2 are reported in Figure S6. In Figure 3, we show the values of the gain coefficients obtained as a function of incident pump intensity. The gain is consistently higher in the case of larger crystals. This allows us to suggest that larger crystals with longer PL lifetimes must be preferred for the realization of lasing devices.

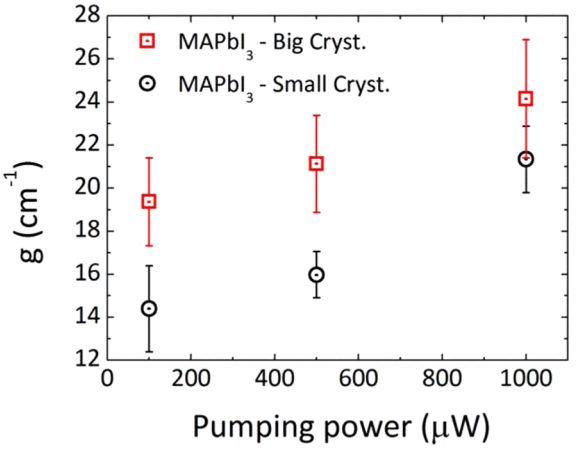

Figure 3. Optical gains for $MAPbI_3$ samples with small crystallites (black circles) and big crystallites (red squares) as functions of pump power. The error bars refer to the 95% confidence intervals of the fitted parameter values.

In conclusion, we have demonstrated that it is possible to design the emissive properties for a single material composition by designing the processing route, which makes solution-

dx.doi.org/10.1021/ja511198f | J. Am. Chem. Soc. 2014, 136, 17730−17733

processable perovskite-based optoelectronic technology even more appealing.

■ ASSOCIATED CONTENT

Supporting Information

Experimental section and top-view SEM images, UV−vis spectra, and cw-PL spectra for all of the investigated samples. This material is available free of charge via the Internet at http://pubs.acs.org.

■ AUTHOR INFORMATION

Corresponding Authors

srinivasa.srimath@iit.it
annamaria.petrozza@iit.it

Notes

The authors declare no competing financial interest.

■ ACKNOWLEDGMENTS

The authors acknowledge funding from the EU Seventh Framework Program [FP7/2007-2013] under Grant Agreement 604032 of the MESO Project. The authors thank Dr. F. Scotognella, Dr. F. Tassone, Dr. G. Grancini, and Prof. G. Lanzani for insightful discussions.

■ REFERENCES

(1) Deschler, F.; Price, M.; Pathak, S.; Klintberg, L. E.; Jarausch, D.; Higler, R.; Hüttner, S.; Leijtens, T.; Stranks, S. D.; Snaith, H. J.; Atatüre, M.; Phillips, R. T.; Friend, R. H. *J. Phys. Chem. Lett.* **2014**, *5*, 1421.

(2) Sutherland, B. R.; Hoogland, S.; Adachi, M. M.; Wong, C. T. O.; Sargent, E. H. *ACS Nano* **2014**, *8*, 10947.

(3) Tan, Z.-K.; Moghaddam, R. S.; Lai, M. L.; Docampo, P.; Higler, R.; Deschler, F.; Price, M.; Sadhanala, A.; Pazos, L. M.; Credgington, D.; Hanusch, F.; Bein, T.; Snaith, H. J.; Friend, R. H. *Nat. Nanotechnol.* **2014**, *9*, 687.

(4) Yamada, Y.; Nakamura, T.; Endo, M.; Wakamiya, A.; Kanemitsu, Y. *J. Am. Chem. Soc.* **2014**, *136*, 11610.

(5) Stranks, S. D.; Burlakov, V. M.; Leijtens, T.; Ball, J. M.; Goriely, A.; Snaith, H. J. *Phys. Rev. Appl.* **2014**, *2*, No. 034007.

(6) Saba, M.; Cadelano, M.; Marongiu, D.; Chen, F.; Sarritzu, V.; Sestu, N.; Figus, C.; Aresti, M.; Piras, R.; Geddo Lehmann, A.; Cannas, C.; Musinu, A.; Quochi, F.; Mura, A.; Bongiovanni, G. *Nat. Commun.* **2014**, *5*, No. 5049.

(7) Manser, J. S.; Kamat, P. V. *Nat. Photonics* **2014**, *8*, 737.

(8) Stranks, S. D.; Eperon, G. E.; Grancini, G.; Menelaou, C.; Alcocer, M. J. P.; Leijtens, T.; Herz, L. M.; Petrozza, A.; Snaith, H. J. *Science* **2013**, *342*, 341.

(9) Grancini, G.; Marras, S.; Prato, M.; Giannini, C.; Quarti, C.; De Angelis, F.; De Bastiani, M.; Eperon, G. E.; Snaith, H. J.; Manna, L.; Petrozza, A. *J. Phys. Chem. Lett.* **2014**, *5*, 3836.

(10) Im, J.-H.; Jang, I.-H.; Pellet, N.; Grätzel, M.; Park, N.-G. *Nat. Nanotechnol.* **2014**, *9*, 927.

(11) De Bastiani, M.; D'Innocenzo, V.; Stranks, S. D.; Snaith, H. J.; Petrozza, A. *APL Mater.* **2014**, *2*, No. 081509.

(12) Ren, Z.; Ng, A.; Shen, Q.; Gokkaya, H. C.; Wang, J.; Yang, L.; Yiu, W.-K.; Bai, G.; Djurišić, A. B.; Leung, W. W.; Hao, J.; Chan, W. K.; Surya, C. *Sci. Rep.* **2014**, *4*, 6752.

(13) Bi, D.; Moon, S.-J.; Häggman, L.; Boschloo, G.; Yang, L.; Johansson, E. M. J.; Nazeeruddin, M. K.; Grätzel, M.; Hagfeldt, A. *RSC Adv.* **2013**, *3*, 18762.

(14) Burschka, J.; Pellet, N.; Moon, S.-J.; Humphry-Baker, R.; Gao, P.; Nazeeruddin, M. K.; Grätzel, M. *Nature* **2013**, *499*, 316.

(15) Docampo, P.; Hanusch, F.; Stranks, S. D.; Döblinger, M.; Feckl, J. M.; Ehrensperger, M.; Minar, N. K.; Johnston, M. B.; Snaith, H. J.; Bein, T. *Adv. Energy Mater.* **2014**, *4*, No. 1400355.

(16) Xing, G.; Mathews, N.; Sun, S.; Lim, S. S.; Lam, Y. M.; Grätzel, M.; Mhaisalkar, S.; Sum, T. C. *Science* **2013**, *342*, 344.

(17) Roiati, V.; Colella, S.; Lerario, G.; De Marco, L.; Rizzo, A.; Listorti, A.; Gigli, G. *Energy Environ. Sci.* **2014**, *7*, 1889.

(18) Cohn, A. W.; Schimpf, A. M.; Gunthardt, C. E.; Gamelin, D. R. *Nano Lett.* **2013**, *13*, 1810.

(19) Jordan, C.; Donegan, J. F.; Hegarty, J.; Roycroft, B. J.; Taniguchi, S.; Hino, T.; Kato, E.; Noguchi, N.; Ishibashi, A. *Appl. Phys. Lett.* **1999**, *74*, 3359.

(20) Stoumpos, C. C.; Malliakas, C. D.; Kanatzidis, M. G. *Inorg. Chem.* **2013**, *52*, 9019.

(21) D'Innocenzo, V.; Grancini, G.; Alcocer, M. J. P.; Kandada, A. R. S.; Stranks, S. D.; Lee, M. M.; Lanzani, G.; Snaith, H. J.; Petrozza, A. *Nat. Commun.* **2014**, *5*, No. 3586.

(22) Yamada, Y.; Nakamura, T.; Endo, M.; Wakamiya, A.; Kanemitsu, Y. *Appl. Phys. Express* **2014**, *7*, No. 032302.

(23) Varshni, Y. P. *Physica* **1967**, *34*, 149.

(24) Knutson, J. L.; Martin, J. D.; Mitzi, D. B. *Inorg. Chem.* **2005**, *44*, 4699.

(25) Filip, M. R.; Eperon, G. E.; Snaith, H. J.; Giustino, F. 2014, arXiv:1409.6478v1. arXiv.org e-Print archive. http://arxiv.org/abs/1409.6478.

(26) Amat, A.; Mosconi, E.; Ronca, E.; Quarti, C.; Umari, P.; Nazeeruddin, Md. K.; Grätzel, M.; De Angelis, F. *J. Nano Lett.* **2014**, *14*, 3608.

(27) Quarti, C.; Grancini, G.; Mosconi, E.; Bruno, P.; Ball, J. M.; Lee, M. M.; Snaith, H. J.; Petrozza, A.; De Angelis, F. *J. Phys. Chem. Lett.* **2014**, *5*, 279.

(28) Filippetti, A.; Delugas, P.; Mattoni, A. *J. Phys. Chem. C* **2014**, *118*, 24843. $R_{rad} = \int_{E_g}^{\infty} \rho_{ph}(\varepsilon)\alpha(\varepsilon)\nu_{ph}(\varepsilon)\, d\varepsilon$ and $n_i = \int_{E_{CBB}}^{\infty} n(\varepsilon)[(1 + e^{(\varepsilon-\mu)/k_B T})]^{-1}\, d\varepsilon$, where α, ρ_{ph}, ν_{ph}, and $n(\varepsilon)$ are the absorption coefficient, photon density of states (DOS), photon velocity, and electron DOS, respectively.

(29) Hangleiter, A. *Phys. Rev. B* **1993**, *48*, 9146.

(30) Stagira, S.; Nisoli, M.; Cerullo, G.; Zavelani-Rossi, M.; De Silvestri, S.; Lanzani, G.; Graupner, W.; Leising, G. *Chem. Phys. Lett.* **1998**, *289*, 205.

(31) Xing, G.; Mathews, N.; Lim, S. S.; Yantara, N.; Liu, X.; Sabba, D.; Grätzel, M.; Mhaisalkar, S.; Sum, T. C. *Nat. Mater.* **2014**, *13*, 4076.